Linking Electrochemistry, Modern Aluminium Cell Design and Operating Conditions, for a Better Understanding of Anode Reactions and Various Levels of PFC Co-evolution

Part 1: Changes in Cell Reactions as Raw Materials and Cell Designs have Evolved.

Barry Welch[1], Mark Dorreen[2] and David Wong[3]
1. Professor, University of N.S.W, Sydney, Australia
1. Consultant, Welbank Consulting Ltd, New Zealand
2. Director, Light Metals Research Centre, University of Auckland, Auckland, New Zealand.
3. Manager Project Delivery & Principal Engineer Environmental, Light Metals Research Centre, University of Auckland, Auckland, New Zealand.
Corresponding author: barry@barry.co.nz

Abstract

Aluminium smelting has always been an evolving process. As a consequence of environmental concerns, control automation, and growth in cell size, there have been changes in the quality of raw materials used as well as changes to the physics of mass transfer within the cell. The alumina shifted from being well calcined "sandy" or "floury" mix of alpha and gamma phases, to one that includes approximately 5 % boehmite (AlOOH), a more stable soluble hydroxide in the electrolyte. Simultaneously there have been increases in sulfur and other impurity levels in the baked anodes. Meanwhile, the volume of the electrolyte in modern cells (per kA) is less than 30 % of what it was, and the area over which the alumina is distributed for dissolution in the cell is reduced also. Better magnetic compensation coupled with the advent of slots in the anodes have also dramatically reduced the driving force for electrolyte mixing introducing spatial variations in cell conditions. The situation is made worse by the longer anodes increasing the travel path for its distribution. Consequently, spatial variations in cell conditions have become more prevalent and with the traditional methods of operation and control of the cells there is an increase in the ease with which PFC co-evolution can occur.

This paper looks at the scientific and practical background of all anodic reactions that can occur and the conditions that contribute to variations in the proportion of each reaction. It simultaneously raises questions on how applicable the past mechanistic interpretations of the anodic processes are, since they have ignored the need to provide the entropic energy of each reaction. With the increase in size of cells, changed cell conditions and work practices, spatial variations can occur more readily and these can have adverse effects on the greenhouse gas footprint. In order to discuss the options to minimise this trend, the understanding of all factors contributing is presented here.

Keywords: Aluminium reduction, anode reactions, gas products, PFC co-evolution, spatial variation.

1. Introduction

The cell design, control, performance and operating conditions of aluminium smelting cells are continuously evolving in order to reduce production costs, minimise the environmental impact, and use the energy more efficiently. Each change brings about a consequential impact, which can affect the basis of the models on which the design and predictions have been based, but at times some of the impacts are overlooked when models are updated. Therefore, the purpose of this

paper is to present a better understanding of what happens within the cell so that models can move from simplifications of the past as the margins of gain have become narrower.

The essential ingredients for aluminium smelting are alumina, a suitable fluoride-based solvent for it, anode carbon and electrical energy. The final stage of the Bayer process for producing smelter grade alumina involves a calcination step to convert the aluminium trihydrate ($Al_2O_3 \cdot 3H_2O$) to the smelter grade product. Originally this was performed by rotary kilns, which have a long residence time, leaving a moisture-free product described as either 'sandy' or 'floury'.

The cell design and operating practices enabled the solvent electrolyte to come in contact with moist air and hydrolyse according to the overall reaction:

$$2Na_3AlF_6(l) + 3H_2O(g) = 6NaF + 6HF(g) + Al_2O_3 \quad (1)$$

which becomes thermodynamically favoured once the temperature exceeds 900 °C. The reacting water could also come from a limited amount absorbed by the non-alpha alumina phases.

The introduction of fluid-bed calcination for aluminas increased the rate of emission of gaseous (HF) and particulate ($NaAlF_4$) fluorides, and the combination of these emissions often upset the ecosystem surrounding smelters and adversely impacting both vegetation and animals. Consequently, hooded cell design modifications were introduced and these were subsequently coupled with dry scrubbing technology. However, coupled with optimising the capture efficiency of the HF, the level of calcination of the trihydrate in the fluid-bed process was reduced in order to provide adequate surface area for efficient HF capture. This resulted in a significant fraction of the Bayer alumina feedstock (~ 5 %) being in the hydroxy-oxide form $Al_2O_3 \cdot H_2O$, which gives rise to a stable hydroxyl anion in the smelter's electrolyte.

Furthermore, the available raw materials and production of anodes have changed over time; anodes today typically have in excess of 2 wt.% S, which can be electrochemically oxidised[1].

With the various changes in smelting cells design, raw materials, work practices and control, new electrochemical reactions are introduced, and these are reviewed here to form a basis for developing better operational and control paths in the future.

1.1. Electrochemical Laws Controlling Parallel Reactions

In electrochemistry the rate of any reaction (i_i) is given by the current carried by that individual reaction and the stoichiometry involved. Where multiple parallel reactions are occurring, the cell current (I_{cell}) is given by:

$$I_{cell} = \sum i_i \quad (2)$$

[1] While there is significant sulfur impurities in the anodes, discussion of reactions involving sulfur are not included in this paper. Practically, it has been shown [1] that it is electrochemically oxidized and released from the anode as COS(g). As it cools and permeates through the crust, it decomposes, giving rise to a range of products including carbon dust, CS_2(g) and elemental sulfur. The proportion that leaves with the anode gas burns to sulfur dioxide in the flame. Analysis of the secondary sulfur reactions shows that they only have a minor impact on the energy balance.

Any reaction where the interfacial potential gradient at the anode E_{anode} is greater than the reversible potential for that reaction, (calculated by the relationship $E_{reversible\ i} = \Delta G_i / nF$) can occur. Thus we have:

$$E_{anode} > E_{reversible\ i} = \frac{\Delta G_i}{nF} \tag{3}$$

Extra energy beyond the reversible value i.e.($E_{anode} - E_{reversible\ i}$) is needed as a driving force to maintain the reaction rate – this is referred to as "overpotential, η_{anode} ". Hence:

$$\eta_{anode} = E_{anode} - E_{reversible\ i} \tag{4}$$

The magnitude of the overpotential to maintain a given reaction rate (hence current density of that specific reaction) can be due to a number of causes, the most common ones being:

- Activation or charge transfer overpotential, for the electrons to transfer between electrode and reacting species.
- Concentration overpotential, where a driving energy is needed to ensure that the reacting ionic species arrive or depart from the electrode surface at the required rate.
    - This often arises through establishing a concentration gradient adding diffusion across a boundary layer to any other natural convective arrival processes.
    - This can also arise through surface coverage of the electrode surface with the product or reaction intermediate. This form of overpotential can lead to passivation.
- Ability to satisfy the entropic energy requirements since the set potential does not necessarily provide the energy required for completion of the overall reaction to the state whereby the products are released.

It must be stressed that for the anode products in the gas to be released, the total interfacial energy transfer must satisfy the enthalpy requirements (ΔH_i) to ensure the product formed is going to be in its released state. Therefore, for each reaction we also have the following relationship that energetically must be satisfied:

$$\Delta H_i = \Delta G_i + T\Delta S_i \tag{5}$$

Thus for reactions where $E_{anode} < \Delta H_i / nF$, extra energy must be provided by means of heat that is transfered to the reaction interface. This requirement has been ignored in the literature generally when discussing mechanisms. (Note: The term $T\Delta S_i$ in equation (5) is sometimes referred to as the "entropic energy".)

1.2. Gaseous Products Identified in Smelting Cells

The consumption of carbon anodes in smelting cells is complex because chemical oxidation by air that ingresses through the imperfect anode covering leads to air-burn, while differential reactivity of the varying structures of carbon also result in particulate detachment of "carbon dust" from the anode. In addition, there is also the impact of the Bouduard reaction that consumes carbon in the reaction with CO_2. Measurements of gas composition evolved below the surface of the electrolyte show the composition varies according to cell conditions and quality of anodes. The ratio of CO_2/CO in well performing smelting cells ranges between 2.4 and 5, but during an anode effect (AE) it changes dramatically to between 0.2 and 0.25 [2]. This happens despite the operating alumina concentration remaining within 5 % of the value it had before the transition, thus showing that the CF_4 co-evolution during an AE is not simply the onset of an independent fluoride decomposition reaction as generally is believed.

Evolution of CF_4 gas plus a surge of gaseous C_2F_6 during the initial part of an anode effect is well known but more recently trace co-evolution of CF_4 under apparently normal (non-AE) operating conditions has become more widespread. The changes in gases and proportions coincide with changes in cell designs, feed materials and operating conditions.

Despite the improvements from dry scrubbing, anode covering and hooding of cells, there are still significant rates of gaseous HF emission from the cell.

1.3. The Enabling and Completion of Chemical Reactions

Using the common convention of setting the cathodic reduction reaction to produce aluminium at zero (0) volt, we can estimate the enabling or reversible potential for each anode reaction after taking into the account the state of the reactants and products using standard, reliable thermochemical databases. The carbon anodes used are heterogeneous composite materials with varying structures but all are based on graphitizable carbon. Therefore, for all reactions involving carbon, graphite is taken as the standard state but the calculated potentials will be towards the upper limit.

Table 1 summarises the calculated electrode potentials and energy requirements for evolution of the various gaseous products when using an electrolyte saturated with smelter grade alumina. The corresponding anode reactions in Table 1 are ranked by increasing reversible potential, $E_{reversible}$, which is the potential to 'enable' each reaction. The "total kJ required" in Table 1 is the total energy required to complete formation of anode products ΔH_i ; some of this is provided electrically by the interfacial potential E_{anode} but the remainder must be supplied by additional heat transfer to the interface ("Q req" in Table 1).

While most of the oxide anions in the melt dissolve as an oxyfluoride complex ion in the melt, for simplicity its role in a reaction is simply represented as O^{2-} since an equilibrium dissociation proportion exists.

Table 1. Energy requirements for anode reactions encompassing products identified in laboratory or operating aluminium smelting cells.

Equation Number	Anode Reaction	$E_{reversible}$ (Volts)	Total kJ Required/mol Al_2O_3 eq*	Q req kW/A·cm² **
(6)	$OH^- + F^- + C = CO(g) + HF(g) + 2e$	0.88	1520	$(26.2-10*E_{anode})$
(7)	$O^{2-} + C + S = COS(g) + 2e$	0.89	1129	$(20.0-10*E_{anode})$
(8)	$O^{2-} + C = CO(g) + 2e$	1.074	1351	$(23.3-10*E_{anode})$
(9)	$2O^{2-} + C = CO_2(g) + 4e$	1.191	1098	$(19-10*E_{anode})$
(10)	$O^{2-} + 2\,F^- + C = COF_2(g) + 4e$	1.85	1438	$(24.8-10*E_{anode})$
(11)	$2O^{2-} + 4\,F^- + 3C = CF_4(g) + 2CO + 8e$	1.8	1530	$(26.4-10*E_{anode})$
(12)	$4\,F^- + C = CF_4(g) + 4e$	2.52	1702	$(29.4-10*E_{anode})$
(13)	$6\,F^- + 2C = C_2F_6(g) + 6e$	2.75	1767	$(30.5-10*E_{anode})$

*Total kJ required/mol Al_2O_3 eq = enthalpy requirements for that reaction, ΔH_i
**"Q req" = the additional energy that must be supplied by heat transfer to the reaction interface, in order for formation of the products to be completed.

Apart from the formation of COS(g) – which has been confirmed independently [1] – each of these reactions have been shown to occur electrochemically using fast sweep voltammetry with a small vertically oriented sulphur-free electrode. Figure 1 presents such a curve, where the carbon anode had low sulphur content; here, the total current across the cell is measured during a rapid sweep of increasing cell voltage (or electrode potential).

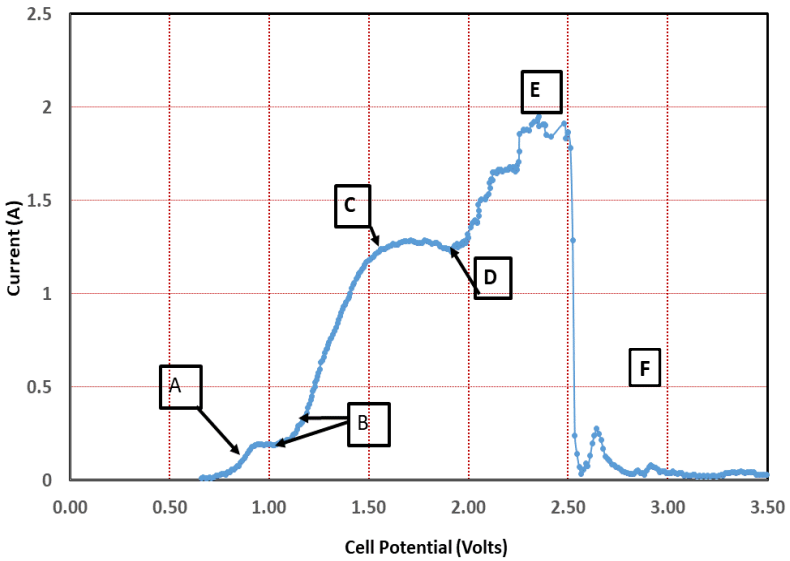

Figure 1. Fast sweep (~ 20 V/s) I-V curve for a smelter electrolyte containing ~1wt.% Al_2O_3.

Current starts to flow in the cell when the cell potential exceeds the value that enables HF to form (0.88 V, as per equation 6). Because of the low hydroxyl concentration in the electrolyte there is rapid onset of concentration polarisation limiting the HF generation (see "A"). However, once the potential exceeds that required for carbon oxides (CO and CO_2) co-evolution (see "B") the current increases as the electrode potential increases – highlighting an acceleration in gas product formation rate occurring – particularly as the potential exceeds that required for CO_2 co-evolution (1.19 V).

The curve also shows the onset of oxide anion concentration polarisation (see "C") induced by the rapid voltage sweep, thereby limiting the rate of current increase until the potential reaches a value ("D") that enables co-oxidation of fluoride anionsthat are present in high concentrations. The current increase continues with the voltage reaching a limiting value (see "E") that is associated with immediate passivation of the electrode surface as can be seen by the virtual instantaneous drop in current after this point. Once the potential exceeds that required for CF_4(g), a limited amount of current passes (see "F"), but then decreases through lack of thermal energy.

1.4. The Role of Heat Transfer

Table 1 highlights there is an interfacial energy deficit (Q req) for sustaining and continuing each reaction unless the applied electrode potential E_{anode} exceeds that given by the relationship $\Delta H_i / nF$.

This energy deficit can only be provided by heat transfer from surrounding materials – either the electrolyte or, in a laboratory cell also the electrode [3]. The ease with which the heat can be supplied in a smelting cell is dependent on the temperature gradient between the electrolyte and the anode surface, and the interfacial heat transfer coefficient. This gradient will be less than the superheat as otherwise electrolyte freeze would occur.

The comparison of the magnitude of the heat required is for an equal reaction rate as given by the same current density for each reaction as illustrated in Figure 2, where the energy gap between the applied potential and that required for isothermal completion comes from heat transferred into the reaction zone ('Q req' in Table 1). The magnitude of the applied potential E_{anode} determines the amount of heat transfer required for each reaction.

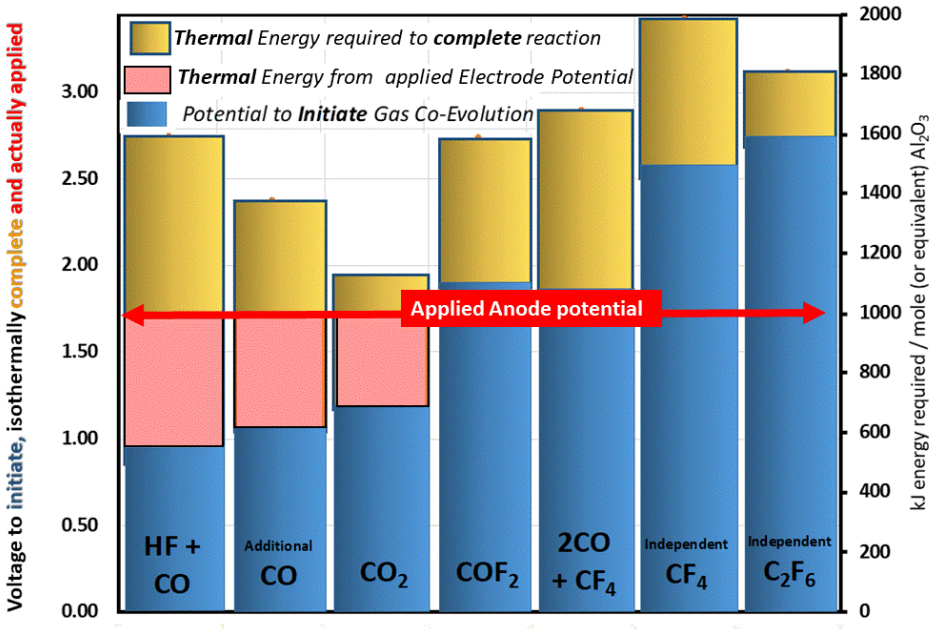

Figure 2. Comparing operating electrode potentials with required to initiate or complete reactions.

A complication linked with the ability for the electrolyte to transfer the required heat to the anode is the competitive heat loss through the anode, the magnitude of which depends on the thermal resistance of the carbon anode and its cover material [3, 4].

1.5. Operating Conditions and Interfacial Anode Potential

The applied anode potential in Figure 2 is shown for illustrative purposes only but is comparable to typical values quoted or assumed in the literature. However, it continuously cycles because of the deliberate modulation of the dissolved alumina concentrations by varying feed rates as part of the control logic. While the amplitude of variation can be typically no more than 50 mV, keeping it in exactly the same band is dependent on consistent performance of the feeders, and on the assumption that all alumina being added is dissolving in the melt. Furthermore, the actual value is difficult to determine as several components that are contributing to the overall cell voltage (such as bubble resistance, electrolyte composition, anode-cathode distance, current density and alumina concentration) are not accurately known nor are they controlled to the required precision.

The average operating cell voltage, $V_{\text{"at cell"}}$, provides the energy for heat loss as well as providing the energy for all reactions. Breaking this voltage down we have the following relationship for the voltage between the anode beam and the cathode collector bars:

$$V_{\text{"at cell"}} = E_{anode} + E_{cathode} + I(R_{anode} + R_{cathode}) + IR_{electrolyte} \qquad (14)$$

Therefore taking the differential of this equation with respect to current can give the instantaneous value for the sum of the anode and cathode potentials. However, this needs to be performed over a

limited current range as the electrode potential has a different dependence on current but simultaneously changes during the current stepping. The commonly used extrapolation method introduces considerable error as the current density increases. Anode changes also cause variation in these parameters.

Model predictions that are sometimes used, are also limited because of lack of knowledge of all the parameters that influence the electrolyte resistance. Cells operating below 200 kA with non-slotted anodes and large anode-cathode distances lead to potential values of approximately 1.65 V. Measurements of the cathode overpotential, which is practically reflected by the concentration of the sodium co-deposited in the aluminium, show that it is typically less than 0.1 V. Best estimates for many of the modern cell technologies indicate that operations are typically with anode potentials closer to 1.75 V. If the interfacial anode potential exceeds approximately 1.8 V (versus a pure aluminium reference electrode), then fluoride anion co-oxidation is enabled (see equations 10 - 11) leading to co-evolution of either the unstable $COF_2(g)$ or extra $CO(g)$ and $CF_4(g)$. One can therefore see that modern cell technologies have little room for movement before anode potentials digress into the zone where PFCs are co-evolved. This also explains why modern cells periodically have very low emission rates of CF_4 .

2. Actual Reactions Occurring in Smelter Cells

2.1. Electrochemical Formation of Gaseous HF Emissions

While the overall dry scrubbing process works efficiently, the change in structural properties of the smelter grade alumina has introduced electrochemical co-evolution as an additional source for gaseous HF. Patterson et al. [5, 6] clearly proved the electrochemical nature of HF generation by adding hydroxyl as NaOH pellets – which introduces hydroxyl ions to the electrolyte of a laboratory cell – and modulating the cell current. Results can best be explained by the following reaction, which coincides with the first peak of the sweep curves presented in Figure 1 (point "A"), i.e. :

$$OH^- + F^- + C = CO(g) + HF(g) + 2e \qquad E_{reversible} \sim 0.88\ V \qquad (6)$$

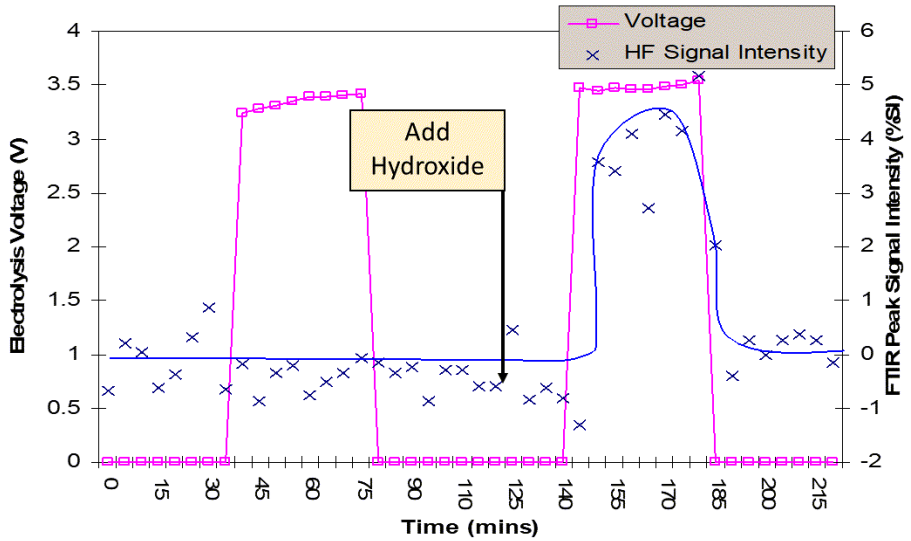

Figure 3. The change in emission rate of HF(g) with and without the current flow and following addition of dissolved OH^- into the melt (added as NaOH).

Figure 4 shows that chemical co-evolution of HF also occurs simultaneously with the electrochemical reaction, since the rate of increase during the alumina overfeed has both an instantaneous and proportional change.

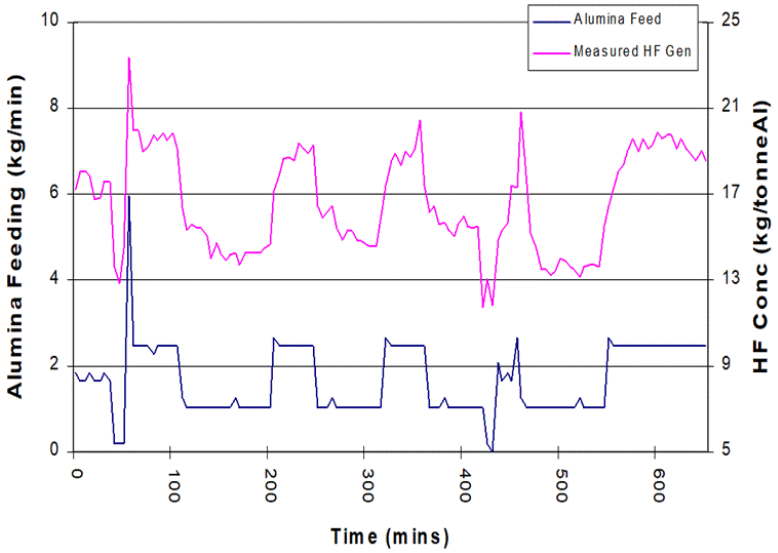

Figure 4. The changing HF evolution rate with changing alumina feeding rate in an operating smelting cell.

2.2. Electrochemical Formation of Gaseous CO

Earlier publications commonly stated that the formation of CO was kinetically inhibited and CO_2 was the primary anode product. The persistence of this interpretation is surprising in view of the earlier publications demonstrating CO free anode gas could never be produced in an operating cell, even when operating at 100 % current efficiency [7, 8].

Laboratory studies we have conducted [9] have shown that at low operating current densities – and irrespectively of the anode quality – CO(g) is electrochemically evolved as the dominant gas. The data presented in Figure 5 is for carefully controlled electrolysis of different quality of anodes classified according to the R&D Carbon reactivity residue measurement. The experimental arrangement minimized the chance that the evolved CO_2 could come into contact with other carbon. However, being performed in an externally heated laboratory cell it will have a much higher driving force for satisfying the entropic heat requirements to the anode irrespectively of current density.

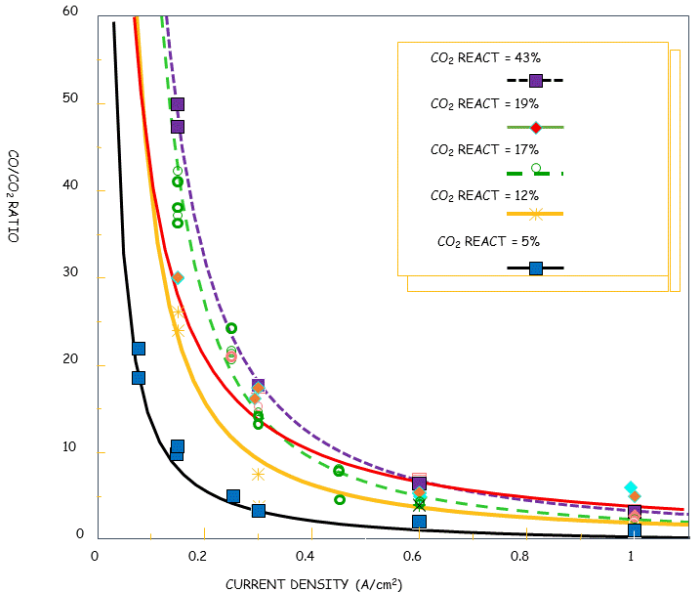

Figure 5. Ratio of carbon oxides (CO/CO_2) evolved at different current densities for anodes of varying quality[9].

The data presented shows the evolved gas has an exceptionally high CO(g) content at low current densities, especially for poor quality anodes (= CO_2 react at 43 %). Usually the high reactivity anodes have been baked at a lower temperature and therefore have a much higher true surface area. However, they also have a more disordered carbon structure.

Of additional relevance are the careful studies conducted by Farr-Wharton [10], who measured the interfacial rate of carbon consumption of vertically oriented, plant produced anodes that later were electrolysed for a fixed number of coulombs ($I \cdot t$) in a laboratory cell. The experimental arrangement ensured minimum gas penetration, thus avoiding an increase in carbon consumption through CO formation chemically. The typical set of results presented in Figure 6 shows that the actual carbon consumption per equivalent decreases approximately by 20 % when the current density increases from 0.3 to 1.0 A/cm^2.

Consequently, these studies confirm that electrochemical formation of CO(g) is occurring at the electrode interface, as per equation 8 or the overall relationship:

$$Al_2O_3 + 3C = 2Al(l) + 3\ CO(g) \qquad E_{reversible} \sim 1.05\ V \qquad (15)$$

This reaction initiates before CO_2 co-evolution starts but it is noted that this reaction is much more endothermic than the CO_2 formation (refer to Table 1 or Figure 2) and it can be constrained by competitive apportionment of the heat being transferred. Thus, if other kinetic conditions are similar, CO_2 formation could dominate. This might be an explanation for some of the misinterpretations in the literature.

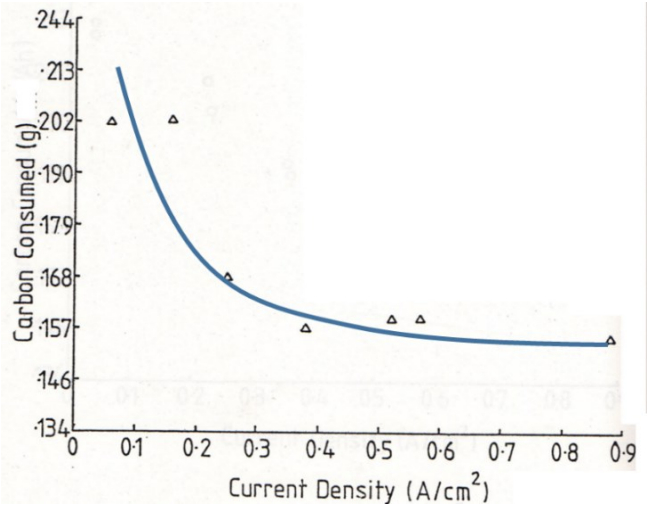

Figure 6. The measured carbon consumption for a fixed number of coulombs, on a vertically oriented anode surface in a laboratory cell [10].

2.3. Chemical Reactions Forming CO Gas

The reaction as represented by the following equation:

$$CO_2(g) + C = 2CO(g) \qquad (16)$$

This reaction,also commonly referred to as the Boudouard reaction, has been shown by both Farr-Wharton [10] and Sadler [11] to occur dominantly in the porosity of the anode immediately behind the anode-electrolyte interface.

In operating cells the flow of gas through anode porosity is driven by the pressure gradient generated by the dense electrolyte and the flow rate tends have a constant value for a given anode quality due to it being constrained by the porosity and near quantitative conversion. Variations in the rate of this reaction for different quality of anodes can be predicted by the “air permeability test” in the models developed by R&D Carbon.

A second chemical reaction giving rise to CO(g) was suggested by Pearson and Waddington [12] to account for some (or all) or of the Faradaic efficiency losses in the smelting cell. They correlated increases in carbon monoxide gas with decreases in current efficiency in smelting cells and proposed the reoxidation of aluminium via the following exothermic reaction, commonly referred to as the “back reaction”:

$$2\ Al(dissolved) + 3CO_2(g) = Al_2O_3(dissolved) + 3CO(g) \qquad (17)$$

Other studies have subsequently shown that this reaction is mass transfer controlled [13] and that the dissolved metal is dominantly solvated sodium [14]. However, with the normal agitation of the metal pad-electrolyte interface, the rate of reaction will be controlled by the saturation solubility of the metal at the interface. Today, the contribution of this reaction to metal efficiency loss is minor because magnetic compensation reduces the mass transfer of the dissolved metal and the use of excess aluminium fluoride lowers the metal solubility.

2.4. Material and Energy Implications of Chemical CO Formation

The oxidising $CO_2(g)$ for both the "Boudouard" and the "back reaction" according equation 17 must be electrochemically generated according to equation (9). Thus we have the following sequence:

$$2Al_2O_3 + 3C = 4Al(l) + 3CO_2(g) \quad (18)$$

$$2Al(l) = 2Al_{(dissolved)}$$

$$\underline{2Al_{(dissolved)} + 3CO_2(g) = Al_2O_3 + 3CO(g)}$$

Overall reaction: $Al_2O_3 + 3C = 2Al(l) + 3\ CO(g)$ (15)

The same applies for the chemically generated CO:

$$Al_2O_3 + 3/2C = 2Al(l) + 3/2CO_2(g)$$

$$\underline{3/2CO_2(g) + 3/2C = 3CO(g)}$$

Adding for the overall reaction: $Al_2O_3 + 3C = 2Al(l) + 3CO(g)$ (15)

Consequently, (and irrespectively of the mechanism whereby the CO(g) is formed), overall the equivalent proportion of metal actually produced is by equation 15 – which requires considerably more energy than if CO_2 was the final product.

2.5. Electrochemical Formation of CO_2 Gas

The difference in the electrode potentials highlighted by the two arrow annotations indicated by annotation "B" of Figure 1 that follow the initiation of CO(g) (as highlighted by the first arrow), approximates to that for enabling the initiation of $CO_2(g)$ at the second inflection marked by an arrow. This gives acceleration in the rate of reaction as the voltage increases suggesting the kinetics of the overall electrochemical reaction is faster than when CO is being formed. This change is also supported by anode overpotential measurements presented in Figure 7. It is interesting to note in that figure the transition from CO(g) to $CO_2(g)$ co-evolution occurs at a higher current density for the increased temperature, suggesting availability of thermal energy plays an important role in determining the proportions of the two gases.

Since it is the same oxide anion being discharged for both CO(g) and $CO_2(g)$, the electrolyte is not in the state of concentration polarisation at the inflexion point, but the kinetics for the release of CO(g) are slower. This could also be due to structural rearrangement necessary to detach the oxygen bonded carbon atom from its solid-state structure. *However within the zone where CO(g) formation is dominant, Figure 7 shows polarisation following the classical shape associated with concentration. The most plausible explanation of this is that there is coverage of the carbon surface with the intermediate surface oxide, thereby effectively increasing current density in the electroactive zone of the electrode.* The steady-state current is established by the rate of release of the oxide matching the rate of oxidation of the anions on the available surface at the effective current density.

The semi-logarithmic relationship between current and overpotential – once CO_2 formation is enabled – is consistent with charge transfer kinetics being the controlling feature until concentration polarisation occurs at the higher current density.

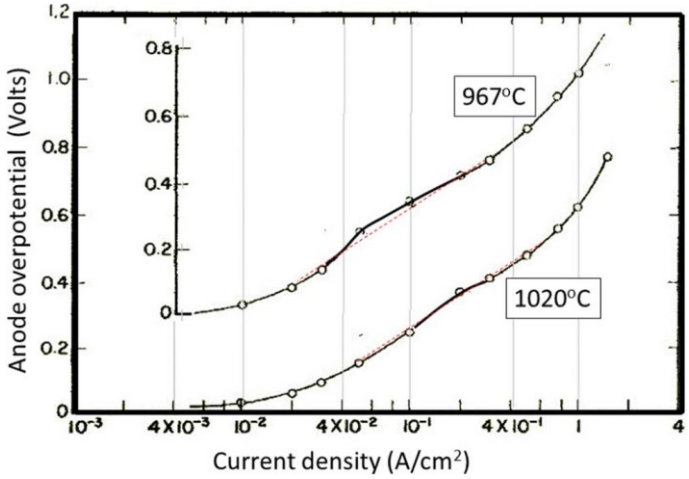

Figure 7. Measurements of anode overpotential in a cryolite-alumina based electrolyte at two different temperatures.

2.6. Electrochemical Co-evolution of CF4 via COF2

Table 1 shows that if the electrode potential exceeds ~ 1.85 V co-evolution of COF_2 can initiate, however, this product can also undergo a chemical reaction with the carbon anode resulting in the net product being a mixture of CO and CF_4 in the proportions 2:1 (discussed in detail later, refer to equation 19).

During laboratory tests for electrochemical depletion of the alumina dissolved in electrolyte using a large horizontally oriented anode (70 to 100 A) for a design that minimizes secondary reactions of the product are minimised or prevented, we have tracked the change in cell voltage and simultaneously performed semi-continuous monitoring of the anode gas using mass spectrometry [4].

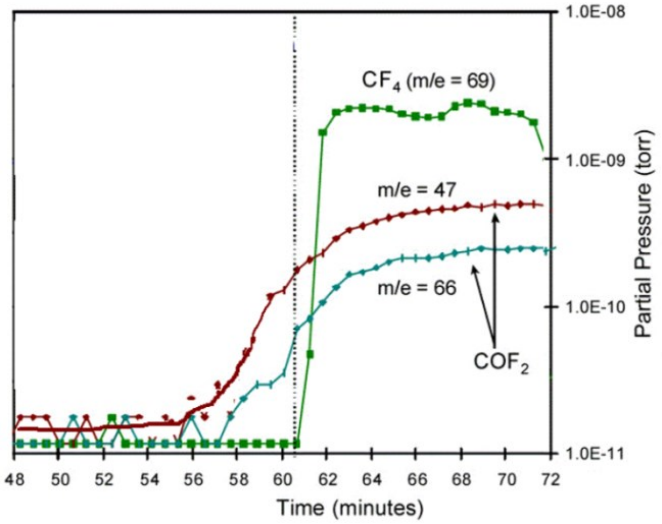

Figure 8. Data showing the onset of PFC co-evolution associated with COF_2 prior to an anode effect [4].

For the current efficiency, operating current, and the electrolyte mass used, the rate of depletion of the dissolved alumina was equivalent to approximately 1wt.% per 15 minutes. Consequently, the data presented in Figure 8 encompasses the depletion of approximately 1.6 wt.% alumina with the anode effect occurring midway through the depletion. The key feature of this data is that co-evolution of COF_2 initiates when the electrolyte has an alumina concentration of ~ 0.4 wt.%

above that needed for an anode effect. During the period leading up to the anode effect the cell voltage increased ~ 0.15 V. Since this increase includes the ohmic contribution of the circuit as it was at constant current, the actual increase in anode interfacial potential through alumina concentration polarization would be less. A significant increase in CF_4 only occurs after the anode effect onset.

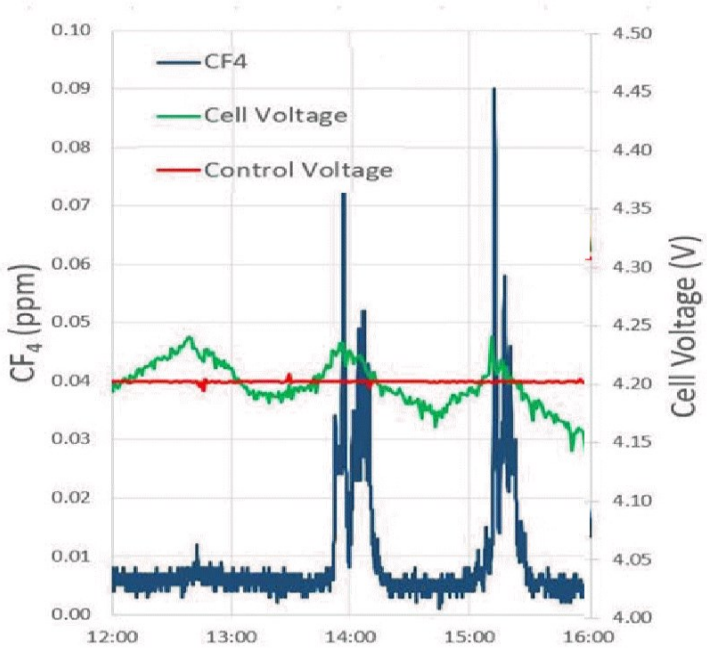

Figure 9. FTIR monitoring of CF_4 co-evolution during "normal" cell operation in an industrial cell.

The data presented in Figure 9 is from a smelter where the alumina concentration is modulated by the normal underfeed/overfeed method as reflected by the green curve. As a consequence of an imbalance between net addition of alumina in the cycle compared with the demand, PFC co-evolution was initiated at the low concentration end of the feed cycle. Thereafter the curve shows a significant and systematic increase in CF_4 concentrations for the small (< 25 mV) changes in anode potential. This attests to the instability of COF_2 in the presence of carbon, decomposing by the thermodynamically favoured chemical reaction:

$$2COF_2(g) + C(s) = CF_4(g) + 2CO(g) \qquad (19)$$

which has a negative Gibbs energy change ΔG of -45.8 kJ at 960 °C. The measured potential increase is too small for any other explanation. Perhaps more important, once initiated this leads to the depolarised reaction proceeds according to equation 11 of Table 1.

3. Transition of Cells to an Anode Effect

Anode Effects (AEs) are not confined to aluminium electrowinning. They have been observed in many molten halide systems and have been induced on carbon electrodes in two different ways depending on the controlling feature of the DC electrical energy supply. When the applied cell voltage is limited or controlled an AE results in a sudden and almost total drop of current. However, if the power supply has constant current control allowing automatic variation in voltage (as occurs with potlines) the voltage increases to a new higher level.

It has been suggested in the literature that an AE caused by either de-wetting or formation of a gas film, but the sudden voltage drop of Figure 1, and other fast sweep publications from Calandra et al. [15, 16] demonstrate that an AE is caused by formation of a passivating, non-conducting, intermediate fluoride-dominated film on the electrode surface.

For fast sweep studies the voltage provides energy for the fast deposition/oxidation of the anion onto the electrode surface. However, if other steps of the overall anode reaction leading to the release of the oxidised product from the surface/reacting zone are *not* completed, this then leads to partial coverage of the electrode surface by reaction intermediates (e.g. C-F surface films). Under steady-state conditions the degree of coverage is determined by the rate of further oxidation matching the rate of release of the surface intermediate. However, the increase in voltage associated with the sweep actually results in an increase in anode potential because of the higher current density. Ultimately this leads to a condition of complete surface coverage by reaction intermediates thereby blocking the current flow. As a consequence, this also stops further heat generation that is needed to satisfy the entropic energy requirements for reaction completion. Hence, passivation can continue with activation energy to drive reaction completion.

In operating smelter potlinese the cells are at or near constant current and upon entering the state of an anode effect, the cell voltage increases to the point where arcing starts occurring in the surface film. This generates sufficient heat for satisfying the entropic energy to complete the transformation from the surface intermediate to the evolved product.

The existence of a fluoride-intermediate film, combined with the high interfacial heat generated during the arcing process at AE initiation, provides a logical and technically sound explanation for the surge in release of C_2F_6 that has been observed [2] in studies involving continuous monitoring of cell gases when anode effects are initiated. As shown in Figure 2, C_2F_6 formation has a lower entropic and overall energy requirement for reaction completion than for CF_4 evolution, even though C_2F_6 requires a significantly higher potential to initiate. This high electrode potential will exist because the electrochemical process can then occur in parallel with the arcing once some of the film is removed.

Figure 10 shows the surge in C_2F_6 evolution that occurs immediately after the onset of an anode effect. However, after the surface film is removed , co-evolution of CF_4 continues in preference to C_2F_6 while voltage remained high and generates substantial heat.The process continues until the alumina concentration increases enough to lower both the anode potential to the required level.

Continuous monitoring of sustained anode effects shows the dominant anode gas becomes CO(g) rather than CO_2. This is illustrated by comparison of the before and anode effect after gas compositions from an operating smelter cell given in Table 2.

The results for various workers encompassing a range of cell technologies the anode gas composition during sustained anode effects shows remarkable consistency with the CO(g) composition typically being in the band of 65 to 70%.

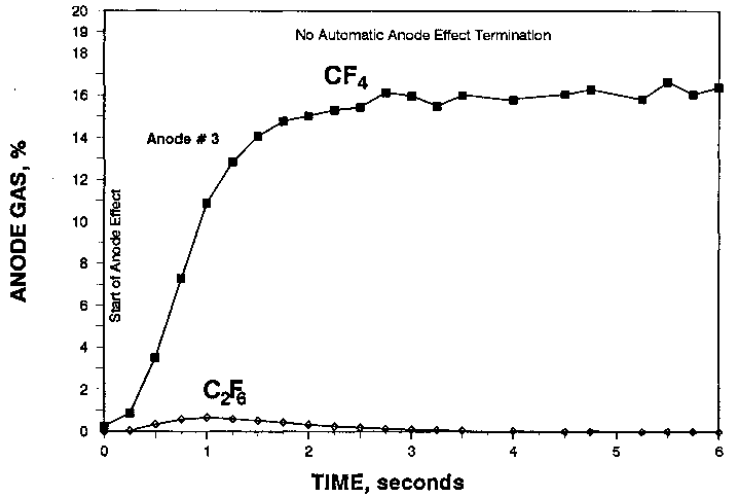

Figure 10. The variation of perfluorocarbon emission rate following onset of an anode effect [2].

Table 2. The change in proportions of chemically and electrochemically generated gases during an anode effect.

Gas	CO_2	CO	CF_4
Gas % Before AE	71	29	0
Gas % after AE	17	67	16
Change	-54	+38	+16
% Current Before AE	83	17	0
% Current After AE	26.1	50.3	23.6

This table also shows the approximate change in distribution of the current between the different reaction products. It is seen that there is a significant increase in the proportion of current being carried by the formation of CO(g) rather than CO_2. One expects with the formation of CF_4 that the proportion of current carried by CO_2 and CO would decrease, however, the observation is that there is a significant increase in CO. The ratio of the extra CO evolved following onset of AE to that of CF_4 is 1.6:1 compared to the expected 2:1 according to equation 11. This is a strong indication that the dominant overall electrochemical reaction is giving rise to the perfluorocarbons even during an anode effect:

$$2O^{2-} + 4\,F^{-} + 3C = CF_4(g) + 2CO(g) + 8e \qquad (11)$$

Reaction 11 initiates at approximately 1.8 V.

The swing in proportions also highlight that while carbon structure plays a role, electrode potential and heat transfer to satisfy the entropic energy strongly influences the composition of the gaseous products.

4. The Link between Theory and Practice!

All studies on both operating cells and laboratory cells show consistency with the analysis presented above, provided that due account is taken of the differences in experimental design or set up such as whether it is externally heated or not, and under current control or voltage control. Electrochemical and thermochemical theory is rigorous and well proven but a modern prebaked anode cell design is at the mercy of humans performing work practices correctly, materials being consistent, and equipment such as alumina feeders working correctly. The cell control strategy assumes the cell conditions enable the alumina to readily dissolve and mix in a homogenous manner while the electrolyte conditions remain unchanged. Figure 11 illustrates the breakdown between theory and practice.

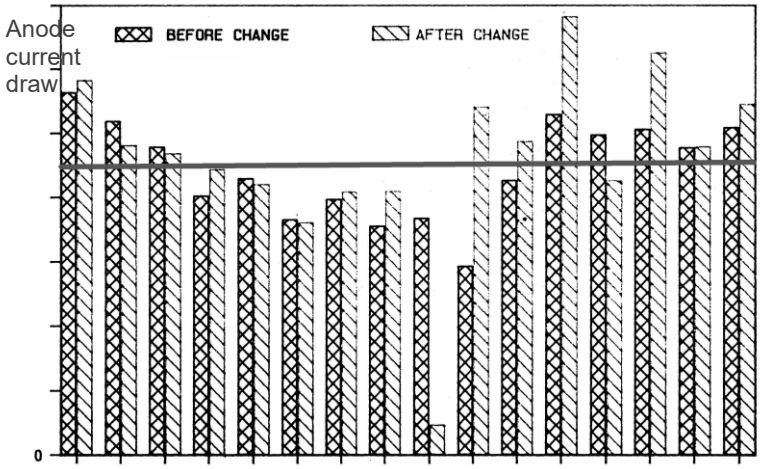

Figure 11. The variation in current distribution between anodes of a cell before and after anode change.

This highlights that industrial cells have spatial variation in conditions. Since there is only a small variation in the anode-electrolyte contact area during the life-cycle of an anode these current changes result in significant variation in the current density and consequently electrode potential. In practice, the temperature always cycles in conjunction with the alumina feeding and control logic as illustrated by the following example that covers 3 hours of operation.

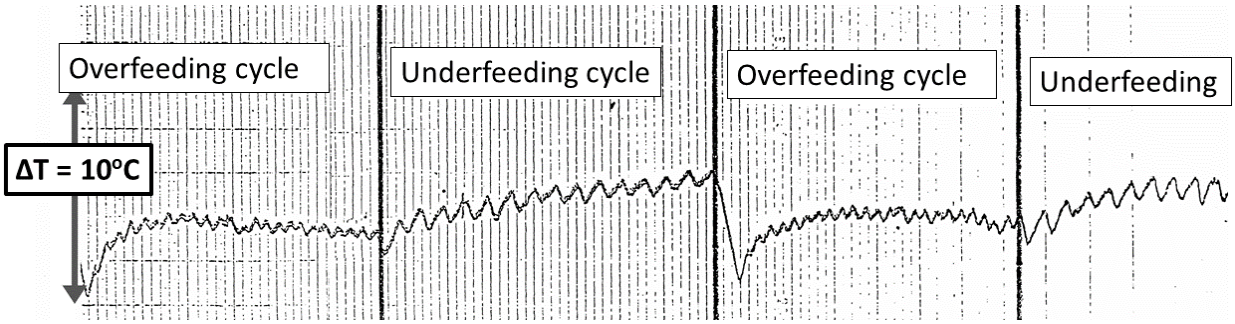

Figure 12. The short term variation in measured electrolyte temperature with feed strategy.

The temperature also varies spatially through the anode change because of the considerable amount of freeze formed on each anode following set. These variations in both temperature and current distribution will result in spatial variations in the interfacial anode potential, and hence proportions of reactions.

4.1. Net Carbon Variation through Anode Quality

We have seen poorly baked anodes have a greater tendency to form CO(g) and this leads to a higher process energy consumption as well as increasing in greenhouse gas footprint.

Mechanistically the following steps would be involved in the overall CO(g) formation reaction mechanism:

$$O^{2-} + xC \rightarrow C_xO + 2e \qquad \text{(Step 1)}$$
$$C_xO \leftrightarrow CO_{(surface)} + (x-1)C \qquad \text{(Step 2a)}$$
$$CO_{(surface)} + Q_{CO} \rightarrow CO(g) \qquad \text{(Step 2b)}$$

where Q_{co} is the magnitude of heat to be transferred in excess of the electrode potential, for completion of CO(g) formation.
In contrast, the following steps would be involved for the formation of $CO_2(g)$ with the first step being the same as the first step for CO formation:

$$O^{2-} + xC \rightarrow C_xO + 2e \qquad \text{(Step 1)}$$

followed by discharge of a second oxyanion onto the same carbon atom as depicted in Figure 13.

$$O^{2-} + C_xO \leftrightarrow (x-1)C^*CO_{2(surface)} \qquad \text{(Step 3a)}$$
$$CO_{2(surface)} + Q_{CO2} \rightarrow CO_2(g) \qquad \text{(Step 3b)}$$

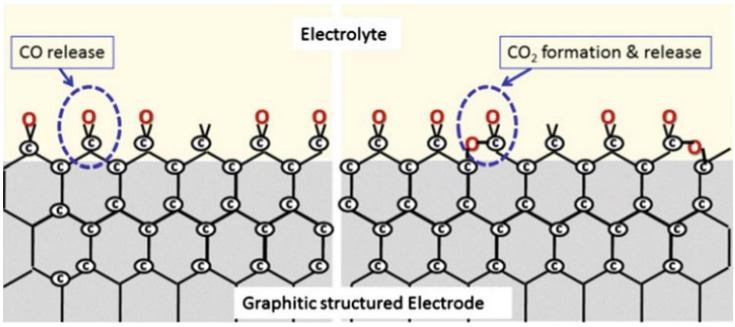

Figure 13. Depicting the difference in bonding structure for CO (left) and CO_2 (right) onto the graphitic surface prior to release as gas.

Taking into account the structure of graphite, kinetically it will be more difficult to break the bonds of the $CO_{(surface)}$ intermediate shown on the left hand side of Figure 13, as compared with the distorted structure of the $CO_{2(surface)}$ intermediate on the right. Hence with lower thermal energy required the overall formation of $CO_2(g)$ should be satisfied faster than CO(g).

However, using the Marsh depiction of the structural variations of carbon in anodes, which varies from some chain-like bonding through to the graphitic structure, some of the carbon atoms will be at a higher thermodynamic activity with less bonding to other carbon atoms – as shown on the left-hand side of Figure 14 as compared to the graphitic structure on the right-hand side.

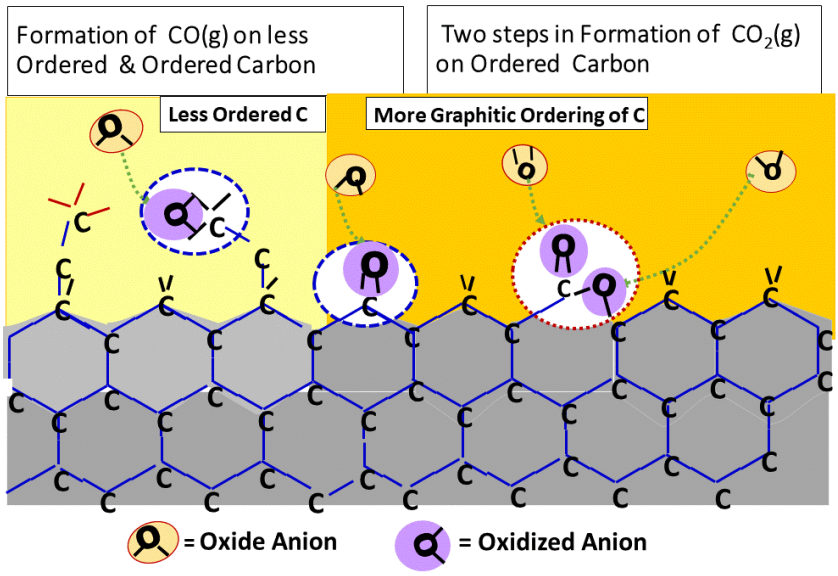

Figure 14. The change in the carbon bonding following electrochemical oxidation of oxide anions onto different structures of carbon.

Following the oxide anion oxidation the poorly structured carbon atom (left-hand side) only has a single bond to fracture during the restructuring process to evolve the gas. In contrast when the oxidised anion is discharged onto the edge of the more ordered graphite structure (central section of illustration), two carbon-to-carbon bonds have to be fractured. Consequently on either energetic or kinetic reasons it is reasonable to expect a slower rate of CO formation at the same anode potential as the carbon is more graphitised.

In contrast, for CO_2 formation two anions are needed to be oxidised by bonding onto a single carbon atom, with the first step being similar to that for CO formation. Discharge of the second oxy-anion automatically involves fracture of a carbon-carbon bond, which will result in a strained structure that requires less thermal energy for conversion to the gaseous phase. Hence kinetically that should be faster than CO formation.

Therefore, while CO formation cannot be prevented, the relative proportion of it can be reduced by having a carbon anode with higher baking temperature, and having a lower heat transfer rate between the electrolyte and anode. And with the reduction one also gets a reduction in energy requirements for operating the cell.

5. Summary and Conclusions

The data presented in the preceding sections highlights several important aspects relating to the environmental and operating performance of modern aluminium smelting cells:

1. Multiple reactions occur at the anode or within the cell. There are a number of contributors to the cause of these reactions:
    a. The quality of the raw materials that are used.
    b. The quality of the work and control practices in adhering to the target operating conditions for the performance intended. And it is noted that different anodes are operating at different current densities and therefore the cells have spatial variability between anodes.
    c. Quality of adherence to the target KPIs such as temperature and aluminium fluoride concentration, operating band of alumina concentration and particularly

the superheat, which influences the resulting transfer between the electrolyte and active anode surface.

2. Critical for environmental performance there is a need to ensure the interfacial anode potential is kept significantly below 1.8 V for all anodes. In order to achieve this:
    a. Conditions need to ensure fast alumina dissolution with good mixing of the electrolyte from the feeders to all the zones of the cell.
    b. The current density of individual anodes is constrained (see below). This is especially so following anode set and the current redistribution.
    c. To minimise the imbalance after anode set, slow anode current pickup to target value needs to be avoided.

3. PFC co-evolution is not confined to anode effects as cells and individual electrodes can continue emitting low levels of CF_4 without any signs of what classically design defines an anode effect.
    a. As a consequence, the present industry definition of an anode effect is too conservative and will result in more significant underreporting of PFC emissions from smelters. Current estimation methods are being updated.

To close, the theoretical development for cell operation and control have been on the assumption that all anodes are behaving the same. Cells operate at constant total current, and under a constrained voltage, which is influenced by the current distribution between anodes and the electrochemical processes occurring at each. While we can get a measure of voltage, we cannot have any measure of the interfacial anode potential, which is one of the two determining factors causing swings in anode reactions and energy efficiency. Spatial variations therefore need to be minimized and then compensated for in some appropriate way in order to optimise the cell's environmental and energy performance.

6. Acknowledgements

The contents of this paper has been generated by an extensive team of co-workers over many years that the authors have been proud to be associated with. Thanks to their efforts we are getting close to completing the jigsaw puzzle. The special thanks to Rod Farr-Wharton, Richard Haverkamp, Edwin Patterson, Alton Tabereaux and Sheryl Hume. And thanks to Halvor Kvande for critical editing and comments.

7. References

1. S.J. Hay, M.M. Hyland, J.B. Metson, E.C. Patterson, M.P. Taylor and B.J. Welch. Electrochemical and Environmental Consequences of Carbon Anode Impurities in Modern Aluminium Smelting Cells *Proc. 7th International Symposium on Advances in Electrochemical Science & Technology*, Chennai, India (2002).
2. A.T. Tabereaux, N.E. Richards and C.E. Satchel, Composition of Reduction Cell Gas during Normal Conditions and Anode Effects, *Light Metals* 1995*,* 325-333.
3. M.R. Dorreen, R.G. Haverkamp, Ali Jassim, N.E. Richards, D.M. Stitt, A.T. Tabereaux and B.J. Welch, Influence of Heat Transfer on Anode Reactions When Electrowinning Metal from Its Oxides Dissolved in Molten Fluorides, *J. Electrochem. Soc.*, Vol. 164, No. 8, H5108-H5118 (2017).
4. M.R. Doreen, M.M. Hyland, R.G. Haverkamp, J.B. Metson, Ali Jassim, B.J. Welch and A.T. Tabereaux, Co-evolution of Carbon Oxides and Fluorides During the Electrowinning of Aluminium with Molten $NaF–AlF_3–CaF_2–Al_2O_3$ Electrolytes, *Light Metals* 2017, 533–539.

5. E.C. Patterson, M.M. Hyland, V. Kielland and B.J. Welch, HF Emissions from Aluminium Cells, *Light Metals* 2001, 365 – 370.
6. E.C. Patterson, Hydrogen fluoride emissions from aluminium electrolysis cells, *Ph.D. Thesis*, University of Auckland, 2002.
7. J.D. Hamlin and N.E. Richards, *Proc. AIME Int. Symposium on Aluminium*, Vol. 2., p. 51 (1962).
8. E.A. Hollingshead and V.A. Braunwarth, *Proc. AIME Int. Symposium on Aluminium*, Vol. 2, 31-50, (1962).
9. S.M. Hume, M.R. Utley, B.J. Welch, and R.C. Perruchoud, The Influence of Low Current Densities on Anode Performance, *Light Metals* 1992, 687-692.
10. R. Farr-Wharton, An investigation into the oxidation of carbon anode competence while subject to electrolysis infused cryolite alumina, *Ph.D. Thesis*, University of N. S. W, Australia, (1980).
11. B.A. Sadler, An investigation into reducing the consumption of carbonaceous anodes during aluminium electrolysis, *Ph.D. Thesis*, University of Queensland, (1989).
12. T. G. Pearson and J. Waddington, Electrode reactions in the aluminium reduction cell, *Discussions of Faraday Society*, Volume 1, p. 307 (1947).
13. S. Gjerstad, and B. J. Welch, The Oxidation of Aluminium by Carbon Dioxide in Presence of Cryolite Electrolyte, *J. Electrochemical Soc*., 111, 976 - 980 (1964).
14. K. Grjotheim, Contributions to the Theory of Aluminium Electrolysis. *Dr. Techn. Thesis*, NTH, Norway (1956).
15. A.J. Calandra, C.E. Castellano, C.M. Ferro, Experimental and theoretical analysis of the anode effect on graphite electrodes in molten sodium fluoride under potentiodynamic perturbations, *Electrochimica Acta,* 25, 201-209 (1980).
16. A.J. Calandra, C.E. Castellano, C.M. Ferro and O. Cobo, Experimental and theoretical analysis of the anode effect in industrial cells, *Light Metals* 1982*,* 345-358.